



HAL
open science

Nighttime morphology of vertical plasma drifts at Ouagadougou during different seasons and phases of sunspot cycles 20-22

B. O. Adebessin, A. B. Rabiou, J. O. Adeniyi, Christine Amory-Mazaudier

► To cite this version:

B. O. Adebessin, A. B. Rabiou, J. O. Adeniyi, Christine Amory-Mazaudier. Nighttime morphology of vertical plasma drifts at Ouagadougou during different seasons and phases of sunspot cycles 20-22. *Journal of Geophysical Research Space Physics*, 2015, 120 (11), pp.10020-10038. 10.1002/2015JA021737 . hal-01302540

HAL Id: hal-01302540

<https://hal.sorbonne-universite.fr/hal-01302540>

Submitted on 14 Apr 2016

HAL is a multi-disciplinary open access archive for the deposit and dissemination of scientific research documents, whether they are published or not. The documents may come from teaching and research institutions in France or abroad, or from public or private research centers.

L'archive ouverte pluridisciplinaire **HAL**, est destinée au dépôt et à la diffusion de documents scientifiques de niveau recherche, publiés ou non, émanant des établissements d'enseignement et de recherche français ou étrangers, des laboratoires publics ou privés.

RESEARCH ARTICLE

10.1002/2015JA021737

Special Section:

Variability of the Sun and Its Terrestrial Impact VarSITI

Key Points:

- Both the PRE and downward reversal peaks exhibit the 11 year sunspot cycle evolution
- A semiannual asymmetry in drift pattern occurred during PRE for all sunspot cycles
- Local presunrise drift enhancement was observed during two sunspot cycles

Correspondence to:

B. O. Adebessin,
f_adebesin@yahoo.co.uk;
adebesin.olufemi@lmu.edu.ng

Citation:

Adebessin, B. O., A. B. Rabiou, J. O. Adeniyi, and C. Amory-Mazaudier (2015), Nighttime morphology of vertical plasma drifts at Ouagadougou during different seasons and phases of sunspot cycles 20–22, *J. Geophys. Res. Space Physics*, 120, 10,020–10,038, doi:10.1002/2015JA021737.

Received 28 JUL 2015

Accepted 20 OCT 2015

Accepted article online 11 NOV 2015

Published online 21 NOV 2015

Nighttime morphology of vertical plasma drifts at Ouagadougou during different seasons and phases of sunspot cycles 20–22

B. O. Adebessin¹, A. B. Rabiou², J. O. Adeniyi³, and C. Amory-Mazaudier^{4,5}

¹Department of Physical Sciences, Landmark University, Omu-Aran, Nigeria, ²Center for Atmospheric Research, National Space Research and Development Agency, Anyigba, Nigeria, ³Department of Physics, University of Ilorin, Ilorin, Nigeria, ⁴UMR 7648, Laboratoire de Physique des Plasmas, Sorbonne Universités, UPMC Université Paris 06, Paris, France, ⁵T/ICT4D, The Abdus Salam International Centre for Theoretical Physics, Trieste, Italy

Abstract The nighttime morphology of vertical plasma drift (V_d) inferred from ground-based measurements of the F layer height at Ouagadougou (12.4°N, 358.6°E) in the African Equatorial Ionization Anomaly trough was investigated. The observation covers four seasons, four sunspot cycle phases, annual, and 11 year sunspot cycle (SC) variations of the SCs 20–22 spanning 1966–1998 and a first attempt of such study. The annual mean peak magnitudes of V_d during the prereversal enhancement (PRE) and minimum reversal periods exhibit the 11 year sunspot cycle evolution with the sunspot number (R_z). The PRE peak/ R_z and reversal peak/ R_z relationships are 98.7% and 84.8%, respectively. PRE peak in June solstice appears 1 h later than for other seasons and is attributed to a decrease in the equatorial zonal wind/conductivity gradient. The highest PRE magnitude and downward perturbation drifts near dusk appear during the equinoxes and lowest in June solstice for all cycles. There is semiannual asymmetry in the variation of V_d during all cycles of the PRE event with peaks in March and September/October. A remarkable feature is the consistent local presunrise drift enhancement for two SCs 20 and 21, which is not a regular feature of the equatorial ionosphere. The rate of inhibition of scintillation effect increases with decreasing phase of sunspot activity and maximizes during the solstices. Both the PRE and minimum reversal peak magnitudes are influenced by the phase of sunspot cycle. Ouagadougou data in this study had shown reliable drift characteristics and can be integrated into the African regional empirical drift model.

1. Introduction

Vertical plasma drift (V_d) is considered as the fundamental factor responsible for the dynamics of the ionospheric F_2 layer [Fejer and Scherliess, 1997]. The drift is the motion of ionized particles at certain altitudes per time, and often involves contributions from neutral atmosphere as well as particle forcing emanating from the actions of gravity, electric, and magnetic fields and gradients. In the equatorial ionosphere, V_d is mainly produced by the activities of zonal electric field with the plasma in the presence of the horizontal magnetic field $E \times B$. At nighttime, the zonal electric field is directed westward (downward reversal), after it must have undergone height intensification (known as the prereversal enhancement, PRE) around the sunset hours. Different driving forces of variability that may emanate from the action of the drift during the evening time PRE had been presented by Santos *et al.* [2013]. Prompt penetration electric field arising from the action of the solar wind magnetosphere and electric field from disturbance wind dynamo had been found to be responsible for the vertical drift variability during the disturbed periods [Rabiou *et al.*, 2007; Abdu *et al.*, 2009; Santos *et al.*, 2012; Adekoya and Adebessin, 2015]. Gravity waves and coupling processes arising from upward propagating planetary waves are dominant during quiet conditions [Abdu *et al.*, 2006]. However, during episodes of the combined magnetically quiet and disturbed conditions, the major source of ionospheric vertical drift variability is the solar flux variations [e.g., Abdu *et al.*, 2010], which has been noted as a key factor in the long-term variation of the ionosphere around the magnetic equator [Ikubanni and Adeniyi, 2013].

Relative to the combined (quiet and disturbed) condition, this paper presents the evening/nighttime morphology of vertical plasma drifts at Ouagadougou, an equatorial station in the African sector during different phases and seasons of the sunspot cycles 20–22, spanning 1966–1998 data sets, with particular emphasis on the PRE peak period and the minimum reversal peak period. These two periods are significant during the nighttime vertical drift investigation [e.g., Adebessin *et al.*, 2013a; Adeniyi *et al.*, 2014a].

PRE essentially accounts for the large F_2 layer uplift and the evening time resurgence of the Equatorial Ionization Anomaly (EIA) and also serves as an indicator/seeding mechanism for the commencement of equatorial spread-F (ESF) or/and scintillation. The effect of the PRE is so strong on the height rise of the evening equatorial F layer by generating steep vertical gradients in the plasma density profile and consequently in the manifestation of ESF occurrence [Sreeja *et al.*, 2009]. Fejer and Scherliess [1997] as well as Martinis *et al.* [2005] had pointed out a strong relationship between the incidence of ESF and the PRE magnitude. Lee *et al.* [2005] had established a direct linear relationship in the magnitude of the PRE and the occurrence probability of ESF. In this paper, the concept of sunspot cycle had been used instead of solar cycle because the solar cycle is more than one sunspot cycle due to the poloidal field reversal.

Several works had been performed at Ouagadougou using the entire three sunspot cycles 20–22 data sets [e.g., Quattara *et al.*, 2009; Quattara and Amory-Mazaudier, 2012; Gnabahou *et al.*, 2013], but not for drift investigations. Some other works done, though not with the entire three sunspot cycles data usage include Adeniyi and Radicella [1998]; Adeniyi and Adimula [1995], and Bilitza *et al.* [2004]. However, the present work is the first detailed study of the variations in plasma drift velocities at this station and in the African sector during three complete sunspot cycles. Ouagadougou is the only African ionosonde station with data set covering three sunspot cycles, hence its choice for the present study. The presentation of this study is divided into four sections. Section 1 introduces the plasma drift and its various drivers during different geomagnetic conditions. Section 2 presents the data and methodology employed. Section 3 is devoted to results and discussions. This composes of investigations into the annual, sunspot cycle (SC) phase, seasonal, 11 year sunspot cycle evolution, validation of Ouagadougou data, and the observation rate of inhibition of scintillation as a function of ionospheric altitude for the entire sunspot cycles 20–22. The last section includes the summary and recommendations, from where our major findings, contribution to knowledge, and final remarks were highlighted.

2. Data and Methodology

Owing to the nonavailability of direct vertical plasma drift measurements in the African sector, most drift observations are inferred using ground-based measurements obtained either from the height of the peak electron density of the F_2 layer, hmF_2 [e.g., Liu *et al.*, 2004; Adebessin *et al.*, 2013b], the virtual height of the F layer, $h'F$ [e.g., Sreeja *et al.*, 2009; Adebessin *et al.*, 2015], or by employing the real height at some fixed frequencies and using the means at such selected frequencies [e.g., Abdu *et al.*, 2004]. Bittencourt and Abdu [1981] and Bertoni *et al.* [2006] had validated the use of inferred drift from ground-based height measurements as near accurate in the absence of direct measurements.

For the purpose of this work, $h'F$ data obtained from Ouagadougou (geographic latitude 12.4°N, longitude 358.6°E, magnetic dip: +1.45) was used to infer the drift, V_d . Adeniyi *et al.* [2014a] and Adebessin *et al.* [2015] had highlighted some physical limitations associated with the accuracy of inferred vertical plasma drifts during the daytime using $h'F$. For this reason, the observations of the present work are limited to the evening/nighttime periods (16–06 LT). The data used span June 1966–February 1998, covering sunspot activity cycles 20–22. The data are made available by the Ecole Nationale Supérieure de Télécommunications de Bretagne (Bretagne) database. The hourly monthly mean of $h'F$ for each nighttime hour (16–06 LT) were computed from the daily values. From these monthly hourly mean values, vertical plasma drift velocities were determined by measuring the time rate of change of $h'F$ (e.g., $V_d = d(h'F)/dt$). Ouagadougou is in the trough of the Equatorial Ionization Anomaly (EIA). The ionosonde at this station is an analogue vertical sounder known as the Ionospheric Prediction Service 42, and composes of a transmitter, receiver, processing, and storage units. For the investigation of the rate of inhibition of scintillation for the entire sunspot cycles 20–22 in section 3.7, daily $h'F$ values around the postsunset period are used. The daily values allow for a better coverage of the event (which is a daily occurrence) rather than the monthly averages.

The Ilorin data (which is used to validate the linear PRE peak/ R_z relationship for regional modeling purpose, as shall be seen later in section 3.5) were obtained from the ground-based DPS-4.2 version Digisonde erected at the Equatorial Ionospheric Observatory of the University of Ilorin, Nigeria. For this station, the drift was inferred from the time rate of change of the height of the peak electron density ($V_d = d(hmF_2)/dt$). The Calculated Average Representative Profile program developed by Huang and Reinisch [1996] was used for the inversion through which hmF_2 was obtained. For more details about the methodology involved in

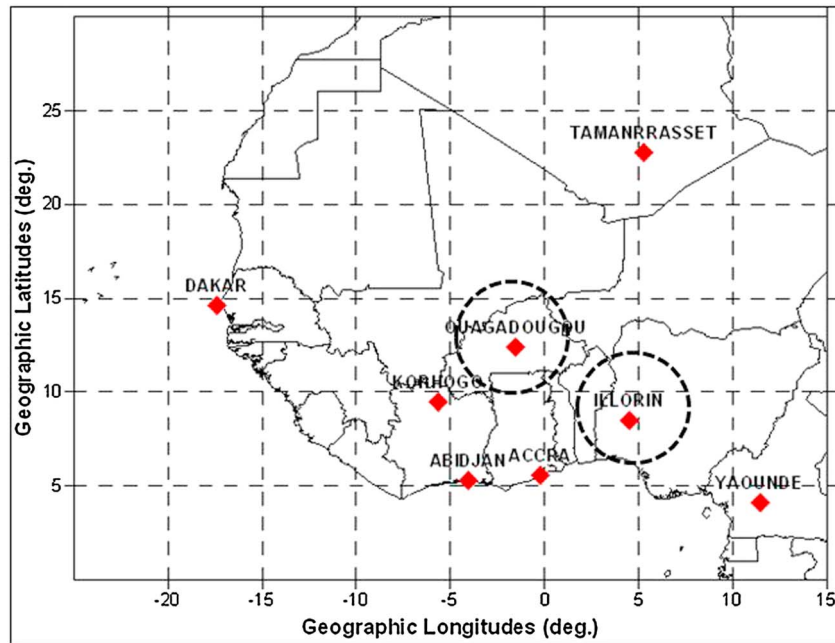


Figure 1. Map showing geographic coordinates of Ilorin and Ouagadougou in the West-African sector—dotted circles (original figure courtesy Obrou [2008]).

obtaining *F* region vertical drift velocities from height profile over Ilorin ionosphere see, for example, Adebessin *et al.* [2013a] and Adeniyi *et al.* [2014b]. The validation of drift inferred using *h'F* at Ouagadougou with that of Ilorin inferred from *hmF₂* observations is made possible because Adebessin *et al.* [2015] had established a similar pattern in the drift obtained from both *h'F* and *hmF₂* observations at a single station at nighttime. In essence, it is not so important whether one uses *h'F* or *hmF₂* to infer the drift at nighttime since both yield similar trend. Figure 1 presents the geographic coordinates of Ouagadougou and Ilorin ionosondes (dashed black circles).

From this point forward, all analyses are based on Ouagadougou data set, except otherwise stated. The seasonal, yearly, sunspot cycle phases, and 11 year sunspot cycle morphology of *V_d* are analyzed. Based on Lloyd's seasonal classification [e.g., Bilitza *et al.*, 2004; Rabiū *et al.*, 2007, 2012; Liu *et al.*, 2010], the months of the year were distributed into three major seasons relative to the position of the subsolar point between the Sun and the Earth, since seasons are actually caused by the tilting of the earth on its axis by about 23.5°. These seasons are June solstice/J-season (May, June, July, and August), December solstice/D-season (November, December, January, and February), and Equinox/E-season (March, April, September, and October). Owing to the significant variations in the equinox months [e.g., Rabiū *et al.*, 2007, 2012], the season is further categorized into March equinox (March and April) and September equinox (September and October). These are the four seasons considered. The sunspot cycle phases and the corresponding years are listed according to the classification by Quattara *et al.* [2009]. The minimum, maximum, descending, and ascending sunspot cycle phases were characterized by $Rz < 20$, $Rz > 100$, $100 \geq Rz \geq 20$, and $20 \leq Rz \leq 100$, respectively. *Rz* is the Zurich sunspot number. For the descending/ascending phases, *Rz* must be less than/greater than the previous year's value. The years (from 1966–1996) that fall into these different categories and with *h'F* data availability are listed in Table 1. Data from 1997 and 1998 are not listed in the table because both years do not fall within the sunspot cycles 20–23, but their values are used elsewhere

Table 1. Years of Different Sunspot Cycle Phases

Solar cycle phase	Minimum ($Rz < 20$)	Maximum ($Rz > 100$)	Descending ($100 \geq Rz \geq 20$)	Ascending ($20 \leq Rz \leq 100$)
20	^a	1968–1970	1971–1976	1966–1967
21	1976	1979–1981	1983–1986	1976–1978
22	1986	1989–1991	1992–1996	1986–1988

^aSC 20 minimum phase year (1964) is not covered by data.

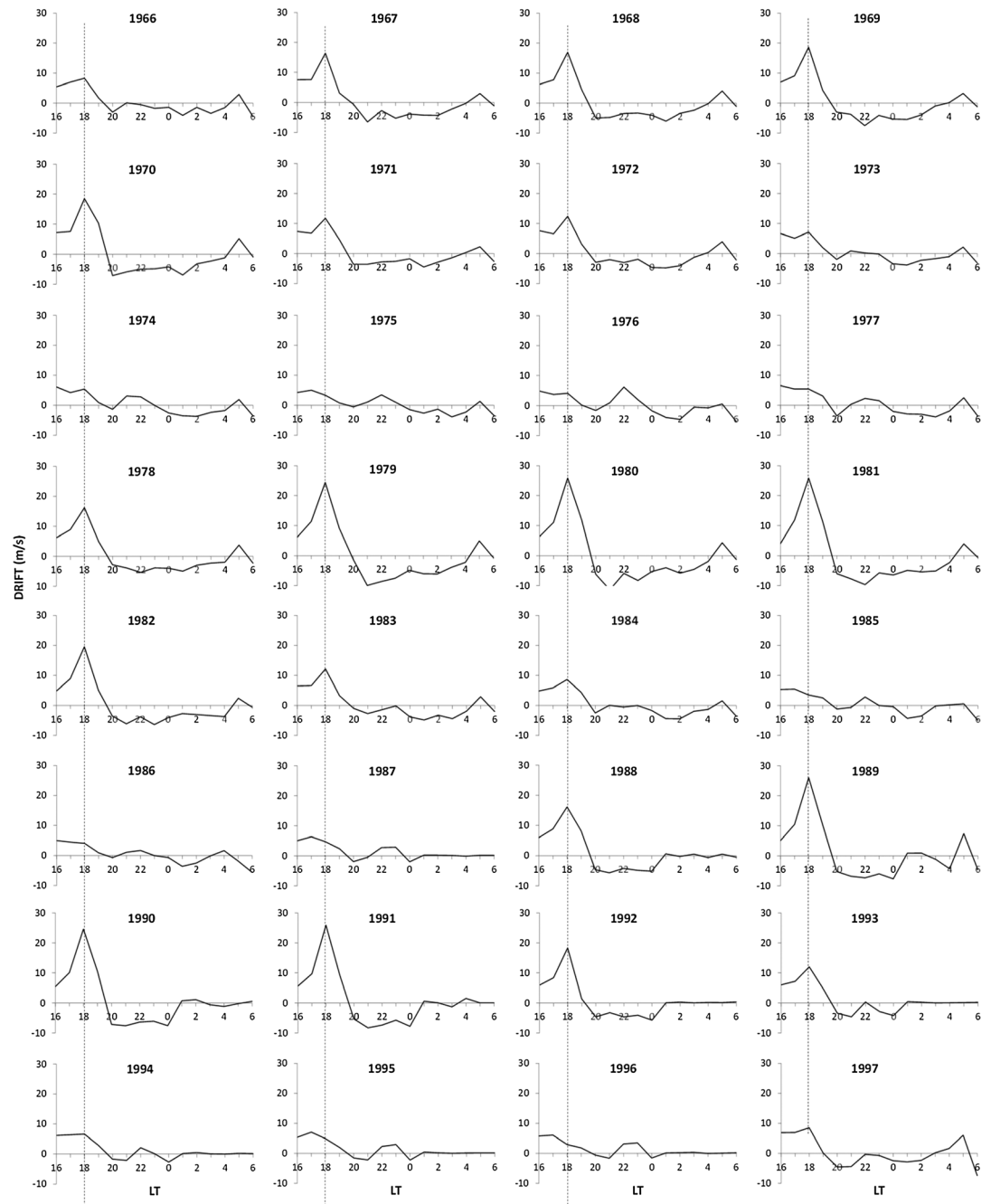


Figure 2. Nighttime annual variation of ground-based inferred vertical plasma drift velocities over Ouagadougou covering 1966–1997. The vertical line across each plot indicates the respective observations at 18 LT (the observation for 1998 is not shown because data were available for only 2 months).

in this paper for other analysis. Further, the minimum phase year, 1964, for the sunspot cycle 20 is not covered by the data under investigation.

Data for the annual Zurich sunspot number, R_z (now the international) is obtained from the National Geophysical Data Centre (NGDC) website at www.ngdc.noaa.gov/stp/spaceweather/solar indices/sunspot numbers. These data are used for the observation of the 11 year sunspot cycle variations during the SC 20–22 relative to the response of V_d during the PRE and minimum reversal peak periods. The international sunspot number substitutes for the Zurich sunspot number in 1981 [e.g., *Klenzing et al., 2013*].

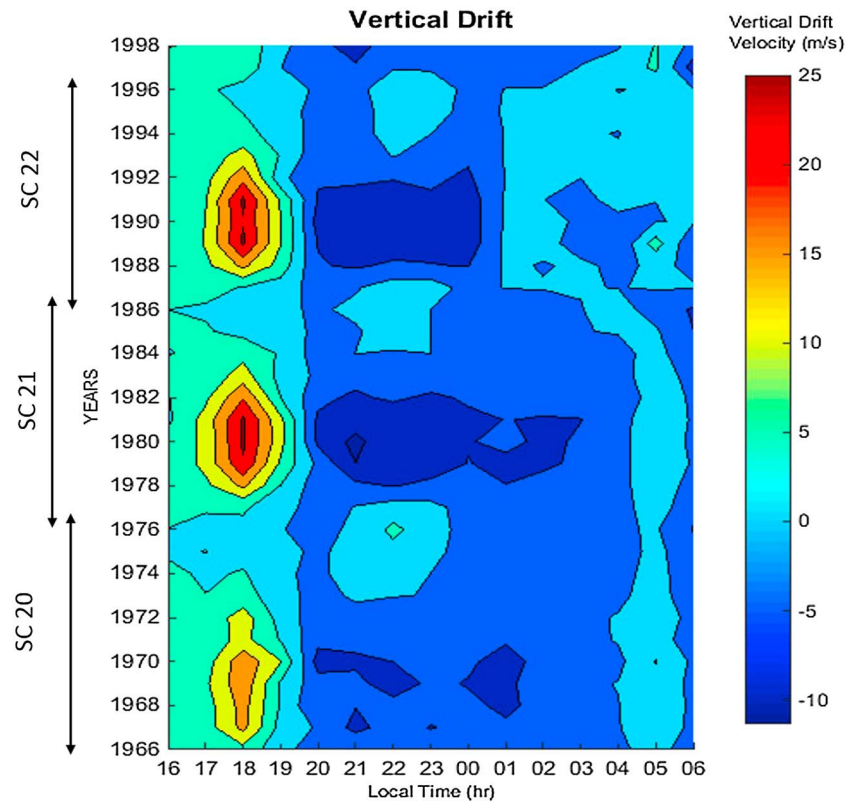


Figure 3. Contour map for all nighttime plasma drift plots in Figure 2.

The following arithmetic developments were carried out:

1. Monthly mean value is the arithmetic hourly daily mean value for a month.
2. Annual mean value (as in Figures 2–7) is the arithmetic hourly monthly mean value for a year.
3. Seasonal mean value is the arithmetic hourly monthly mean value of the months constituting a particular season in a year.
4. Sunspot cycle seasonal mean value (as in Figure 5) is the arithmetic hourly monthly mean values for months constituting a particular season covering the entire years (11 years) that made up the sunspot cycle.
5. The 11 year cycle monthly PRE/minimum reversal peak mean values (as in Figure 6) is the arithmetic hourly monthly mean value for similar months present in all 11 years that constitute a sunspot cycle during the PRE/minimum reversal periods. For instance, for the month of January during SC 20, the mean is the monthly mean values of all data sets during the PRE/minimum reversal periods in January 1966–January 1976, same for February, March, and so on.
6. The sunspot cycle phase mean value (as in Figure 10) is the arithmetic hourly mean values of the years that constitute a particular cycle phase per sunspot cycle event (as listed in Table 1).
7. The minimum reversal peak magnitude is the maximum negative value of the plasma drift.

3. Results and Discussion

In this section, we initially investigate the annual nighttime pattern of plasma drift over Ouagadougou ionosphere and see its effect on the height profile. Then, we examine the seasonal, 11 year sunspot cycle evolution trend, and variations for different solar cycle phases. Next is the validation of the linear PRE peak/ R_z relationship using the data obtained from Ilorin ground-based measurement. Finally, we report the statistical variation of the inhibiting characteristics of the drift to scintillation effects using $h'F$.

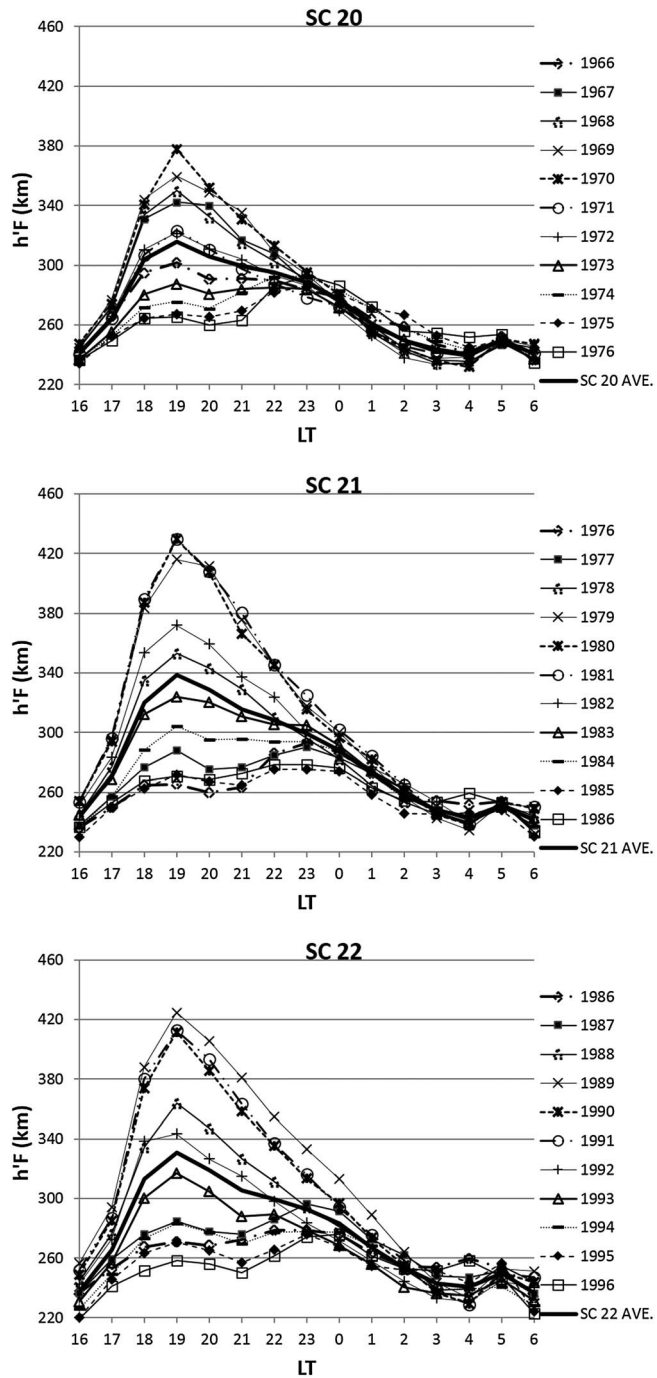


Figure 4. Nighttime annual profile of $h'F$ over Ouagadougou ionosphere for sunspot cycles 20 (first panel), 21 (second panel), and 22 (third panel).

3.1. Annual Nighttime Drift Pattern Over Ouagadougou

The hourly annual nighttime variation of the inferred plasma drift velocities (V_d) for the entire years (1966–1997) over Ouagadougou are presented in Figure 2. Each activity year is characterized by an evening time enhancement (PRE) and immediately followed by a reversal. The emergence of the PRE (the influx of a postsunset peak in upward plasma drift) is a pointer to sudden faster electron depletion from the equatorial ionosphere. It is worth mentioning that the apparent upward movement of the equatorial F layer is a consequence of the actions of both the eastward electric field and the recombination effects of molecular species at the F layer

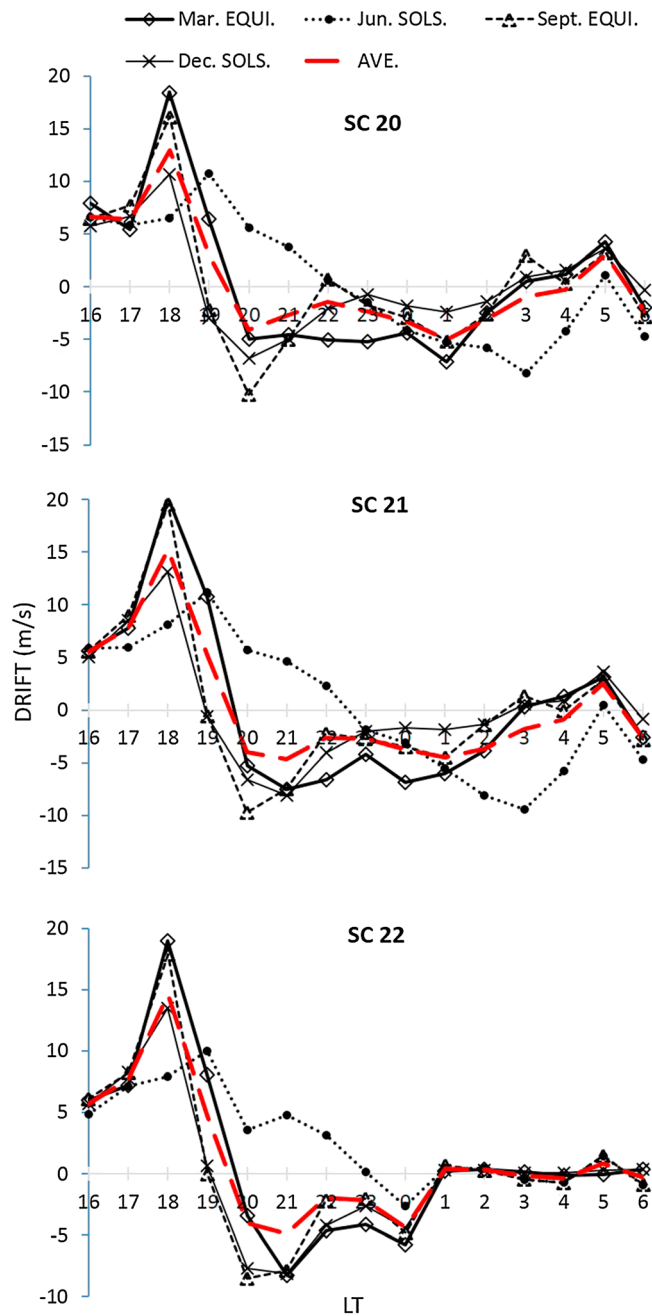


Figure 5. Nighttime average seasonal variation of drift pattern for sunspot cycles 20–22. March equinox is represented by open diamond, June solstice by black circle, September equinox by open triangle, and December solstice by open cross. The red colored dashed line on each plot is the average sunspot cycle variation for each corresponding cycle.

bottom side (or height of reflection), whereas the electric field action controls the downward movement during the postsunset hours. Detailed physical explanation on the nighttime plasma drift morphology can be obtained from one of our previous works [see Adebesein *et al.*, 2013b].

Generally, PRE peaked around 18 LT except for some few years, for example, 1975–1977, 1985–1987, and 1995–1996. Some other fascinating features were also observed.

1. The first feature is the normal nighttime morphology of drift during a successive combination of a year before and after the maximum phase period during all sunspot cycle activities (e.g., 1967–1971 for the

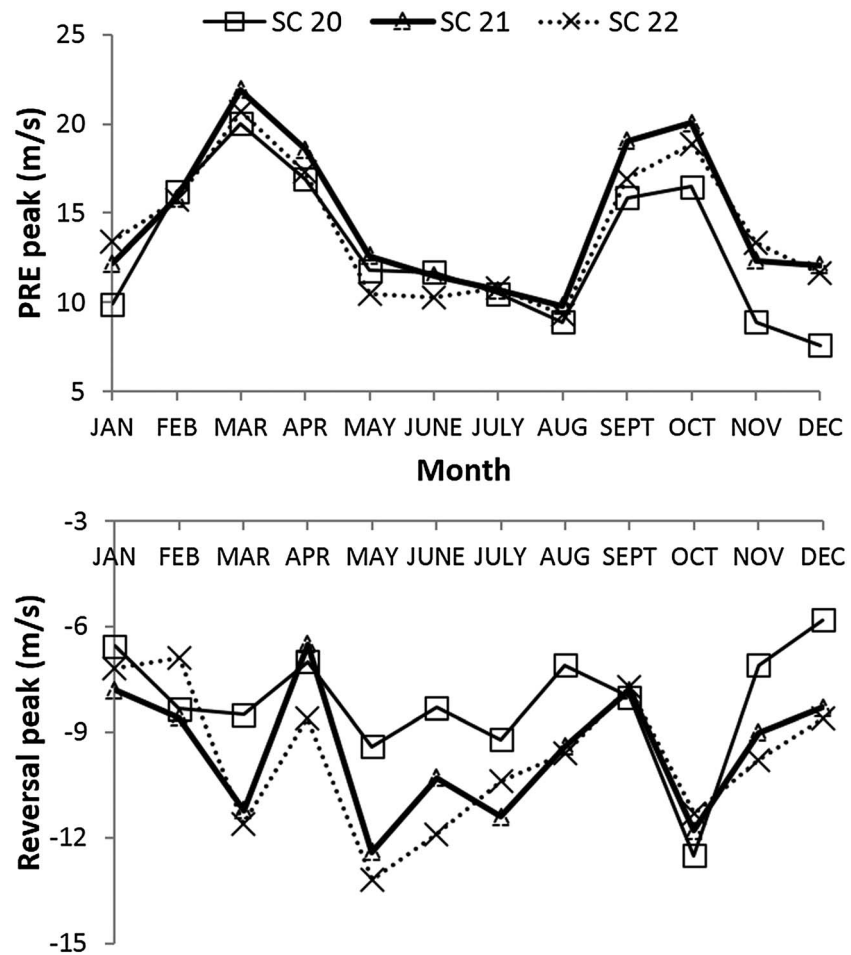


Figure 6. Average monthly variation of vertical plasma drift for SC 20–22 during (top) maximum PRE and (bottom) minimum reversal peak periods.

sunspot cycle 20, 1978–1982 for cycle 21, and 1988–1992 for cycle 22). Under this condition, the minimum reversal peak magnitude was reached immediately after the PRE period.

- The second is a successive yearly increase in the drift velocity at 22 LT during some of the years that constitute part of the descending phase for each of the sunspot cycle event (e.g., 1973–1976, 1984–1986, and 1993–1996 respectively for SCs 20–22). It is worth mentioning that during these (descending) phases, there are more activities related to high-speed solar wind speed flowing from the coronal holes [Zerbo *et al.*, 2012] and therefore the reason for the increase in the drift magnitude as observed.
- For other years in SCs 20 and 21 (i.e., 1966–1986), there is an enhancement in the drift pattern around the presunrise hour (~05 LT) followed by a downward excursion.
- The fourth feature is an insignificant/marginal drift pattern between 1987 and 1996 (except 1989) of the SC 22 spreading around the postmidnight hours of 01–06 LT. The different patterns exhibited in 1989 during this period may be connected with the high geomagnetic activity that characterized the year—these are the severe geomagnetic activities of 14 March, 19 September, and 21 October 1989 with respective magnetic index (*Dst*) minimum peak magnitudes of -589 nT, -255 nT, and -268 nT [e.g., Adebisin, 2008]. Further, theoretical investigations have shown that during geomagnetic activity, the disturbance winds have a tendency to positively charge the nighttime equatorial ionosphere and consequently producing the largest electrodynamic effects in the post-midnight sector [Richmond *et al.*, 2003; Fejer *et al.*, 2008].

The presunrise enhancement characteristic in the third feature above is not a regular feature of plasma drift in the morning local time of the equatorial ionosphere. This feature is observed to be driven by zonal electric field created as a consequence of the polarization field which develops from the actions of thermospheric wind and

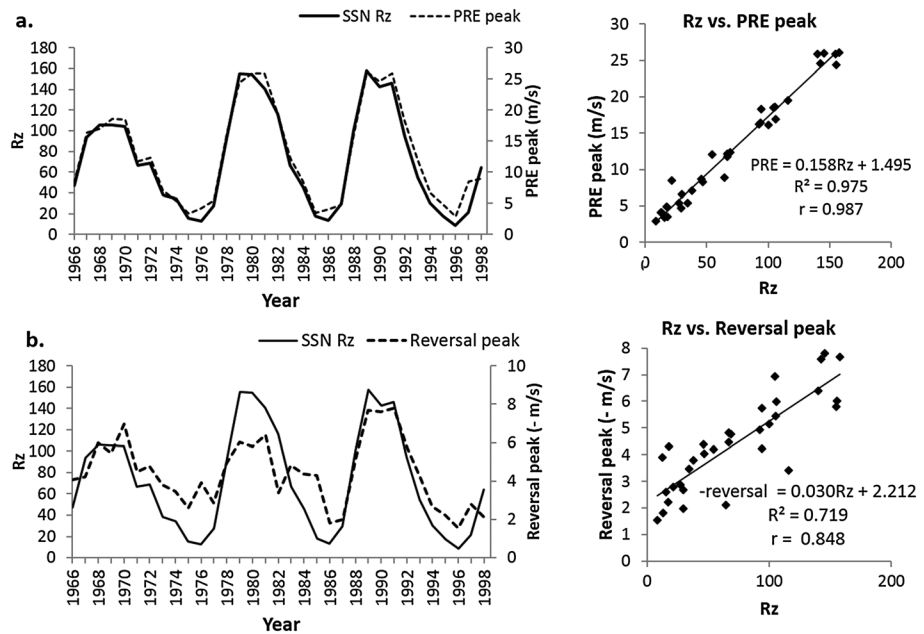


Figure 7. Nighttime yearly average variation of solar sunspot number Rz (solid line) with vertical drift pattern for the entire sunspot cycles 20–22 during (a) peak PRE (dotted line, right) and (b) minimum peak reversal (dotted line, right) periods. The linear equations and correlation coefficients are shown on the pane of each figure on the right-hand side.

steep conductivity gradients in the E region [Nayar *et al.*, 2009]. Around the sunrise period, the electric field initially builds for a short period and consequently increases the conductivity rate in the E region. This effect creates vertical velocity pattern as a result of the additional interacting effect of both the E and F layers, which can only be present near the local sunrise terminator, creating related abnormal characteristic in the drift pattern [e.g., Rishbeth, 1971]. Nayar *et al.* [2009] had reported similar feature using the HF Doppler radar and Digisonde to characterize plasma drift at Trivandrum (8.33°N, 77°E, and dip 0.4°N) in the Indian sector.

The observations in Figure 2 are further processed for clarity by using the contour map in Figure 3. PRE peak magnitudes (around 18 LT) and minimum reversal magnitudes (between 20 and 01 LT) were observed during the maximum phase periods of the SCs 20–22 with that of SC 20 lower than others. The presunrise enhancement (around 05 LT) was clearly shown for SCs 20 and 21, but absent during SC 22.

3.2. Ionospheric Height Profile at Ouagadougou

The nighttime annual profiles of $h'F$ over Ouagadougou ionosphere for the three sunspot cycles are highlighted in Figure 4. On the average, $h'F$ altitudes are relatively high during SCs 21 and 22 compared to SC 20. Height increase was observed during the postsunset period attaining maximum around 19 LT. This shows that the plasma drift which peaked about an hour before (from Figure 2) around 18 LT is actually responsible for the heightening of the F layer altitude. For the high-solar activity years in the three SCs considered, the increase of the F layer height was observed above the 300 km threshold value [see Adebisin *et al.*, 2013a] during the evening time observations. Even for the lower altitudes of the $h'F$ profile during minimum-/low-solar activity conditions, the brisk transformation in $h'F$ pattern generally points toward the effects of electric field perturbation. The presunrise enhancement characteristic is also visible here, though smaller in magnitude compared to the evening time observation. An interesting feature here is that the presunrise enhancement starts about an hour earlier (i.e., 04 LT) for two of the sunspot minimum years considered (1986 and 1996). At any sunspot cycle, there is height increase with increasing sunspot activity [e.g., Adebisin *et al.*, 2014].

It is worth mentioning here that though some earlier works [e.g., Bittencourt and Abdu, 1981; Sreeja *et al.*, 2009] had stipulated the 300 km threshold value for ionospheric F layer altitude as a condition for the vertical drift velocities obtained from Digisonde measurements to be equitable/match the vertical $E \times B$ drift, as determined by direct Incoherent Scatter Radar (ISR) measurements. It was however observed that most of such works were considered for sunspot maxima periods. On the contrary, the derived drift observations

of November 2007–October 2008 (a period of sunspot minima) by *Uemoto et al.* [2010] showed that the virtual height ($h'F$) profile used for their drift derivation was often less than the 300 km and yet a good comparable result. *Abdu et al.* [1981a] had also inferred drifts from $h'F$ observation for the months of June, September, and December 1978, as well as April and June, 1979 at Fortaleza with $h'F$ altitude values well below the 300 km magnitude especially between the evening/nighttime periods of 15–18:30 LT and 23–06 LT with well-established results.

Additionally, *Rishbeth* [1981] and *Adebesin et al.* [2013a] had submitted that the lifting of the ionospheric F layer above the 300 km altitude may not be sufficient enough a condition to trigger the Rayleigh-Taylor instability mechanism, though necessary. It can therefore be suggested that the drift velocity inferred from the ionosonde measurements for any height magnitude below 300 km (just as is seen occasionally in the $h'F$ plots of Figure 4) can be regarded as a virtual representative of the real vertical $E \times B$ measurement in the absence of any chemical correction (since direct measurements are not available). For this reason, the use of the nighttime $h'F$ data at Ouagadougou F region is justified.

The only likely limitation to the method of obtaining drift velocity from F layer height magnitude less than 300 km is the underestimation of the real $E \times B$ drift magnitude [e.g., *Bittencourt and Abdu*, 1981].

3.3. Seasonal Drift Pattern Over Ouagadougou for SCs 20–22.

Figure 5 depicts the average seasonal observations of plasma drift for each of the solar cycle events, with the average response indicated by the red dashed line for each set of observation. Four distinct remarks are noticeable. (1) There is an equinoctial maximum and solstitial minimum in the PRE peak magnitude for all SC events. This is because the conjugate point mapping is most effective in equinoxes and therefore maximizes during this period [e.g., *Adeniyi et al.*, 2014b]. (2) The peak PRE magnitude during June solstice (which is also the smallest) peaked an hour after, relative to other seasons for all SC activities. (3) The minimum reversal peak value for all seasons peaked between 20 and 21 LT, except during June solstice, in which this peak was identified around 03 LT, especially during SCs 20 and 21. (4) There is a disappearance in the bulge that was created around the presunrise (05 LT) period as one moves away from SC 20 toward SC 22, and (5) For all seasons except June solstice, there are appearance of larger downward drifts near dusk immediately after the PRE period.

The real phenomena responsible for the appearance of the smallest PRE peak magnitude in June solstice (in the second remark), for each of the sunspot cycle event, are to some extent an open question, and the major physical rationale for it is yet to be fully understood. Despite this, the characteristic can be attributed to the slow growth rate of the Rayleigh-Taylor (R-T) instability mechanism during the season (June solstice). It is well known that both the thermospheric zonal wind and the longitudinal/local time in the Pederson Hall conductivity across the terminator control the magnitude and time of commencement of PRE [e.g., *Su et al.*, 2009]. However, PRE magnitude will be largest when the magnetic meridian and the sunset terminator are almost aligned at a given longitude [*Adebesin et al.*, 2013a, and the references therein]. The magnetic declination angle is a major parameter that determines this alignment [*Abdu et al.*, 1981b]. Consequently, for the negative magnetic declination angle over Ouagadougou longitude, it is expected that the minimum alignment condition will be in June solstice, leading to a delay in the F layer altitude. It is worth mentioning that the average magnetic declination angle over Ouagadougou for the cycles 20–22 are -7.38°E , -6.18°E , and -4.11°E , respectively, changing by 0.10, 0.13, and 0.11°E per year in similar order (see www.ngdc.noaa.gov/geomag-web/ for the magnetic calculator).

The maximum PRE magnitude which peaked 1 h later in June solstice than for other seasons for all sunspot activity cycles (20–22) is as a result of decrease in the equatorial zonal wind and conductivity gradient. The decrease causes delay in the zonal drift reversal, and as such the PRE peak during this season is dragged further into additional time. Further, the delayed peak can still be considered as a residue of the actual PRE which is supposed to be present around the 18 LT that other seasons peaked, but failed to activate due to higher conductivities (like the blanketing Sporadic-E) in the conjugate E regions that peaked around the same time that PRE magnitude should have maximized.

Another likely factor for the discrepancies observed during June solstice is the plasma density irregularities in the F region equatorial ionosphere, which starts around the dusk and midnight hours of June solstice [*Oyekola*, 2011, and the reference therein]. *Li et al.* [2011] had reported high-equatorial F region irregularities (EFIs) during the postmidnight hours of June solstice for high solar activity period in the African sector. This postmidnight EFIs were suggested to be a spillover effect of the postsunset EFIs.

Table 2. Correlation Coefficient for the Variation Between Sunspot Cycle Index and Plasma Drift Observations

Sunspot cycle	Rz versus PRE peak	Rz versus Reversal peak
20	0.992	0.849
21	0.994	0.757
22	0.993	0.989
All	0.987	0.848

Figure 6 presents the average monthly variation of the drift for SCs 20–22 during maximum PRE and minimum reversal peak periods. Semiannual asymmetry was observed in the monthly variation of the drift for the three sunspot cycle events during the PRE period (Figure 5, first panel) with first peak in March and

the second in September/October. This observation is consistent with the monthly evolution pattern of f_oF_2 over Ouagadougou using similar time span (1966–1998) presented by Quattara *et al.* [2009], as well as the drift pattern presented by Adebessin *et al.* [2013b] using the 2010 ground-based ionosonde data at Ilorin. The major causes of the semiannual anomaly as suggested by Rishbeth *et al.* [2000, and the reference therein] are the neutral air composition changes evolving from the large scale thermospheric dynamics, changes in atmospheric turbulence, inputs from atmospheric waves, and variations in geomagnetic activities. The difference in the drift pattern is more pronounced during SC 21 and least in SC 20, especially from September through January. Further, the PRE drift magnitude during the solstices is higher in December solstice (November–January) than in June solstice (May–July) for SCs 21 and 22, while the reverse is the case for SC 20. It is worth noting that the difference in the drift magnitude between December solstice (higher) and June solstice (lower) as a consequence of the redistribution of plasma between the two seasons is what gives rise to the December/winter anomaly—see Rishbeth and Garriott [1969].

For the minimum reversal peak magnitude (second panel), the asymmetry is not so distinct, though characterized by comparable pattern with varying magnitudes during the three cycles. The difference in the observed magnitudes is attributed to the differing time of attaining minimum peak value during the reversal period, which ranges between 00 and 03 LT for the entire months. For this reversal event, the highest minimum peak magnitude occurred during SCs 21 and 22, while the lowest occurred during SC 20.

3.4. 11 year Sunspot Cycle Evolution

A principal characteristic of the Sun is the 11 year periodicity cycle/variability. These variations are the exact outcome of varying strengths of solar discharges. Fejer [2002] had highlighted various modulating factors of the low-latitude evening prompt penetration electric fields and submitted that both the response time of initialization and the steady state leakage of high-latitude electric fields into the ionospheric evening time low latitude is solar cycle determined. In this section, the 11 year solar activity progression is compared with the drift pattern. Presented in Figure 7 are the respective superimposed yearly vertical drift observations and the corresponding yearly solar sunspot number (Rz) evolution during the PRE peak period (Figure 7a, right) and the minimum reversal peak (Figure 7b, right) period. To the right of each plot are the corresponding plots of the linear equations and correlation coefficients between the observed parameters.

The annual averages of each of the evening time PRE and minimum reversal peak magnitudes of the drift correspond reasonably well with the solar sunspot number Rz . The correlation coefficient r for the entire three 11 year SCs evolution is 0.987 and 0.848 for the PRE peak versus Rz and reversal peak versus Rz observations, respectively. The linear equations are as shown on each pane of the figures. We observe higher-slope magnitude for the PRE peak/ Rz relationship (0.158) than for the minimum reversal peak/ Rz connection (0.030). Further, Table 2 highlights the correlations between the same set of observations for each of the three SC periods. There is no significant difference in r for the Rz /PRE peak observations for SCs 20–22. However, the Rz /reversal peak relationship exhibits the highest/lowest during SC 22/21. This implies a better relationship between the solar sunspot number and the minimum reversal peak magnitude during SC 22 than for other cycles.

The higher-correlation magnitudes observed for the plasma drift/sunspot number relationship (for PRE and reversal periods) are in a way attributable to the source through which the drift is inferred, which is the F layer base height ($h'F$). This is consistent with the average correlation value for the $h'F/Rz$ which is higher than that of the $h'F_2/Rz$ correlation observation for the same set of data (1966–1998) reported by Quattara *et al.* [2009]. Quattara *et al.* [2009] had attributed the single dependence of the virtual height ($h'F$) to only the toroidal solar magnetic field component as the major reason for the higher correlation they observed, whereas $h'F_2$ depends on both the toroidal solar magnetic field components (UV/EUV sources) and the poloidal components. While the

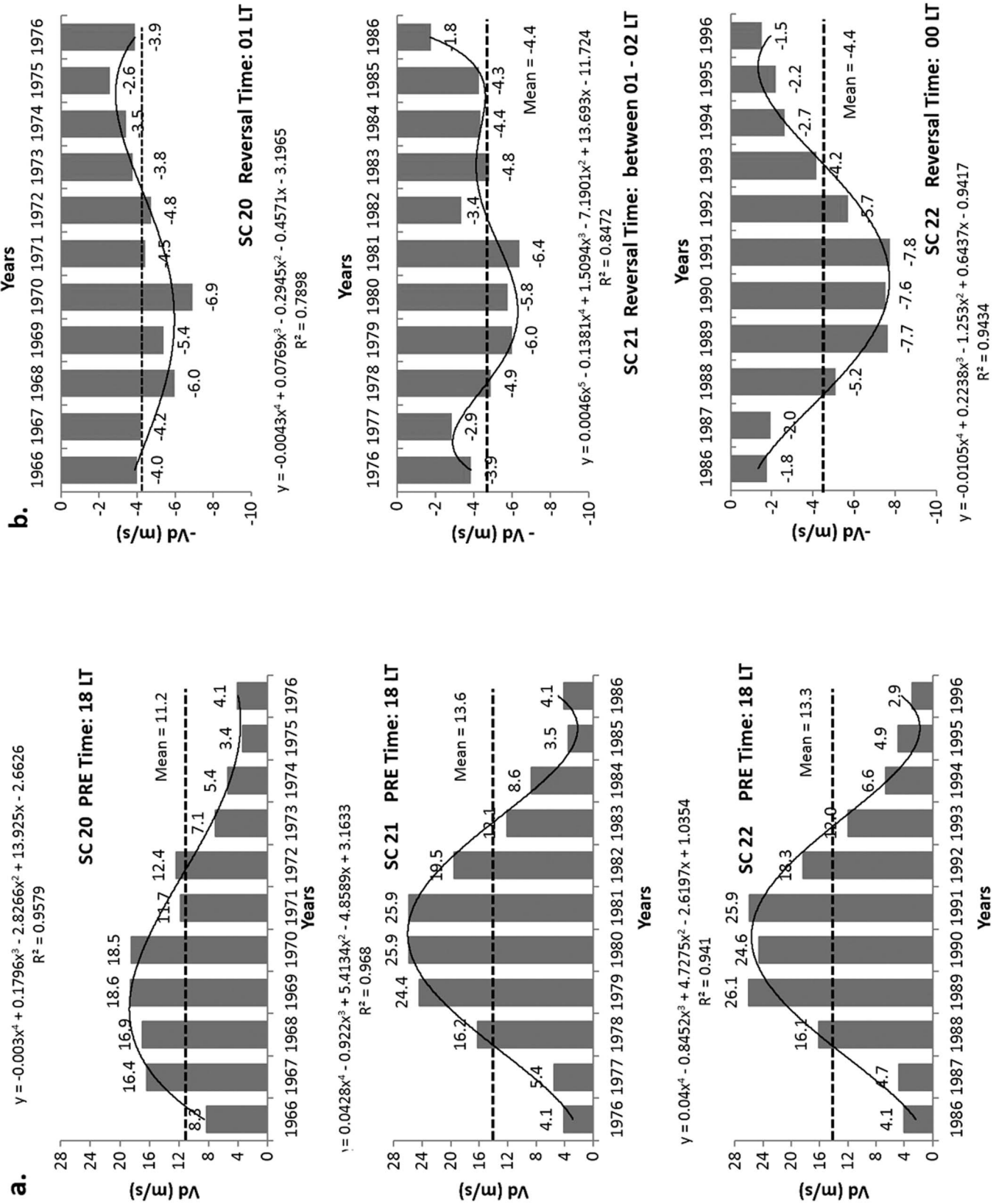


Figure 8. Bar chart showing the average yearly response of (a) the PRE and (b) the minimum reversal peak magnitudes during sunspot cycles 20–22 (inset are the fourth-order polynomial equations and regression magnitudes).

Table 3. Monthly Mean PRE Peak Magnitude of Plasma Drift Velocities Obtained Over Ilorin F_2 Ionosphere for a Low Solar Activity (LSA) Year 2010 Covering March–December (Data Obtained From Adebessin *et al.* [2013a])

Month	PRE peak magnitude (m/s)
March	10.2
April	4.2
May	−1.1
June	3.1
July	−1.0
August	2.6
September	5.1
October	3.5
November	7.8
December	8.0

toroidal solar magnetic field controls the sunspot behavior, the poloidal solar magnetic field controls the solar wind behavior [Simon and Legrand, 1989]. Both the PRE and minimum reversal magnitudes increase with solar cycle. Further, while the poloidal field which are high-speed solar wind streams flowing from coronal holes constitute about 91.5% of geomagnetic activities, toroidal field on the other hand, which are shock events from coronal mass ejections presents only about 8.5% of geomagnetic activity.

The observation is further buttressed with the bar chart in Figure 8. The figure highlights the average yearly response per sunspot cycle

event during the PRE and minimum reversal peak observation periods. Insets are the yearly average magnitudes for each activity. In Figure 8a, the mean PRE peak magnitude for SC 20 is 11.2 m/s and increases during SCs 21 (13.6 m/s) and 22 (13.3 m/s). The average yearly response during the reversal period (Figure 8b) on the other hand recorded approximately equal values (−4.4 m/s) for each of the sunspot cycle event. In addition, while the average PRE peak time is 18 LT for all sunspot cycles, the minimum reversal on the average peaked at 01 LT, 01–02 LT, and 00 LT for the SCs 20–22, respectively. Further, the continuous thick curve covering each of the bar charts is a representative of the highest regression magnitude one can obtain for each set of years comprising corresponding sunspot cycles. For each of the SC activity period in Figures 8a and 8b, the pattern/trend of variability between the years of each activity is best represented by the fourth-order polynomial equation (except for the minimum downward peak value during SC 20 whose highest regression fit was the fifth order polynomial) with regression values greater than 0.80. Recall that there is a better correlation fit for both the PRE peak/ R_z and reversal peak/ R_z relationships. It can therefore be suggested that the 11 year sunspot cycle for SCs 20–22 are of the fourth-order polynomial pattern. The implication/relevance of the pattern of the fourth-order polynomial in Figure 8 is that the pattern can be used as an indicator for modeling the trend of plasma drift during the PRE and reversal peak periods. This is left open for further studies, especially for those in modeling ionospheric parameters.

3.5. Validation of Ouagadougou Data Using the Annual Mean Magnitude During PRE Period

The result from the annual mean magnitude of the plasma drift for each of the years under investigation at Ouagadougou (Figure 7a) was validated for accuracy in modeling purposes, by comparing with the ground-based inferred drift over Ilorin F_2 ionosphere for the sunspot minimum year 2010 with solar radio flux index, $F_{10.7} = 81$ solar flux unit. Ilorin (latitude 8.50°N, longitude 4.68°E) is another equatorial station in the African sector whose drift characteristics/patterns were recently studied by Adebessin *et al.* [2013a, 2013b] and Adeniji *et al.* [2014a, 2014b], and F layer/electrojet characteristics by Adebessin *et al.* [2013c]. The validation for Ouagadougou drift data is achieved by comparing the values obtained from the summation of the monthly mean values of V_d during PRE peak period over Ilorin for the year 2010 (which is not presented in the present work) with that of the linear equation obtained from the peak PRE/solar sunspot (V_d/R_z) relationship over Ouagadougou (Figure 7a correlation plot). Table 3 presents the monthly mean PRE peak values over Ilorin for March–December 2010. Data were not available for January and February.

At Ilorin, the summation of the PRE peak values for all months divided by the total number of months denotes the annual PRE peak magnitude.

$$\text{This implies that} \quad \text{annual}_{\text{Ilorin}} \text{PRE peak} = 4.2 \text{ m/s} \quad (1)$$

Using the PRE peak/ R_z linear equation obtained from Figure 7a at Ouagadougou,

$$\text{peak PRE} = 0.158R_z + 1.495. \quad (2)$$

In 2010, annual R_z is 16.5;

$$\text{hence,} \quad \text{peak PRE} = 0.158 (16.5) + 1.495 = 4.1 \text{ m/s} \quad (3)$$

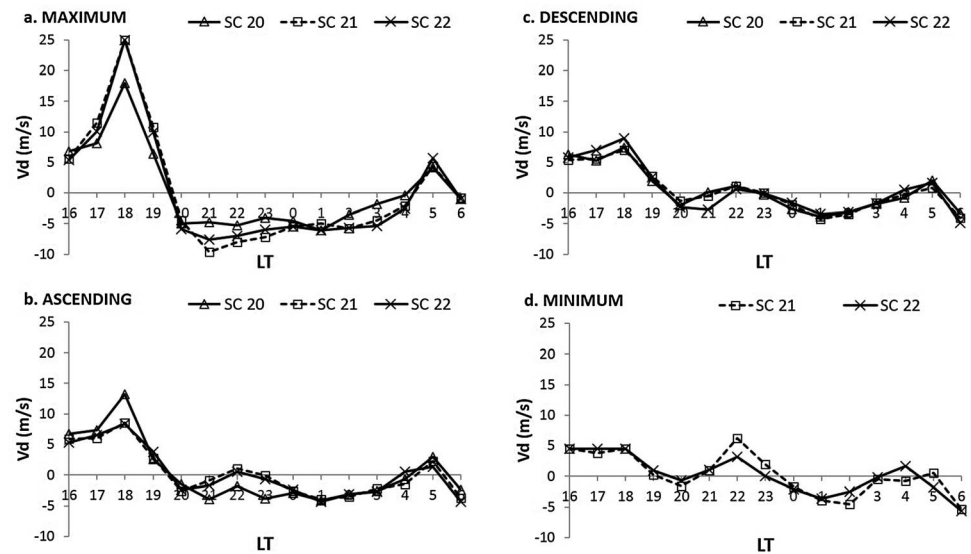


Figure 9. Hourly mean values of vertical plasma drift observations during (a) maximum, (b) ascending, (c) descending, and (d) minimum phase periods of the sunspot cycles 20–22.

In this sense, both values from equations (1) and (3) are very similar. It therefore follows that the linear drift expression obtained for Ouagadougou for the peak PRE/Rz relationship in equation (2) can be used to predict the annual PRE peak magnitude for stations along the EIA trough in the African sector (see Figure 1) provided the corresponding annual solar sunspot number for that year is known.

3.6. Drift Observations During Different Phases of SC 20–22.

In this section, the consideration of the four sunspot cycle phases (i.e., maximum, ascending, descending, and minimum) implies that the influence of the sunspot cycle is taken into account. Figure 9 presents the nighttime hourly mean magnitudes of V_d for the different phases of SCs 20–22. Figure 9a is for the maximum phase or high sunspot activity (HSA) period. Figure 9d is for the minimum phase or low sunspot activity (LSA), while Figures 9b and 9c respectively represent the observations for the ascending and descending phases or together as the moderate sunspot activity (MSA) condition. The entire four sunspot phases with corresponding years are as listed in Table 1. From the entire Figure 9, the following characteristics were apparent: (1) both the PRE peak magnitude and the minimum reversal peak magnitude decreases as the solar sunspot activity phase decreases for the entire three SCs, (2) the drift magnitude between 21 and 22 LT is highest at sunspot maxima, being obvious during SCs 21 and 22 than SC 20, (3) a depletion in the variation was observed around the presunrise (05 LT) period as the sunspot activity phases decreases from maximum through minimum, (4) during the maximum phase, SCs 21 and 22 recorded higher PRE magnitudes than the SC 20, (5) similar pattern was observed for the entire SCs during the ascending and descending phases, probably because both phases are in the MSA period, and (6) the PRE magnitude relative to other hours is almost insignificant during the minimum phase period (the observation for SC 20 is not shown as the R_z for the years in SC 20 used in this work exceeds our classification for sunspot minimum).

The PRE magnitude (in observation 6) which is almost insignificant/low during the minimum phase period of the entire sunspot cycles 20–22 is as a consequence of the corresponding reduction in the equatorial zonal wind and conductivity gradient [Adebesin *et al.*, 2013a, and the reference therein] and subsequently results in the decrease of F region heights. The last statement is consistent with the height profile observation in Figure 4, in which case the altitude is lower than the 300 km height level during the low sunspot activity years for each of the SCs.

It therefore follows from these observations that the sunspot cycle phase is a factor to be considered in characterizing the magnitude of the PRE and minimum reversal peaks. The higher the sunspot cycle phase, the higher the magnitudes of the resultant plasma drifts, and vice versa. A striking feature is the local time presunrise (05 LT) plasma drift enhancement, as explained earlier in section 3.1, and its magnitude is sunspot cycle phase dependent, just as the evening-time PRE. Observations from the Incoherent Scatter Radar (ISR) data had indicated that the evening-time upward and nighttime downward drift decrease from solar sunspot maximum through minimum [Fejer, 2002], whose variability is local time and solar cycle dependent.

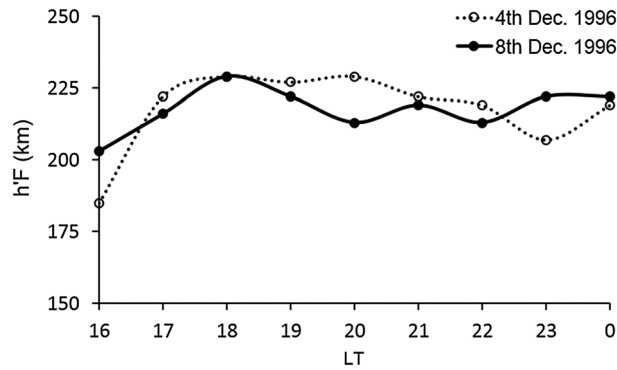


Figure 10. Two samples of condition/pattern for determining the inhibition characteristics from the height profile ($h'F$).

3.7. Inhibition of the Likelihood of Scintillation Effect as a Function of Ionospheric Altitude During the Entire Sunspot Cycles 20–22

The irregular structures in the ionospheric plasma distribution often regarded as scintillation can have a profound effect on the signals of radio frequency if not properly monitored. However, scintillation effect occurs more rapidly around the magnetic equator owing to plasma instability mechanisms (R-T mechanism). Here the inhibition of the likely occurrence of scintillation (or/and spread-F) based on the heightening of the ionospheric F layer

height profile ($h'F$) is considered. As earlier mentioned in section 1, the evening-time PRE of the eastward electric field is responsible for the increase in the ionospheric F layer height around the postsunset period. This height increase subsequently serves as a seeding mechanism for the evolution of spread-F and hence scintillation [e.g., Fejer and Scherliess, 1997; Martinis et al., 2005; Lee et al., 2005]. However, during certain occasions in the low-latitude ionosphere, the dynamo electric field caused a drift away from the F layer, thereby instigating the plasma drift to decrease. Under this condition, the F layer height will not increase appropriately, and in turn the production/appearance of scintillation will be inhibited. In essence, the postsunset increase/decrease in $h'F$ has been observed to be an indirect measure of the seeding/inhibiting characteristics to the existence of scintillation effect in the ionospheric region [Mazaudier and Blanc, 1982; Mazaudier et al., 1984; Kelley et al., 2009].

As mentioned in the methodology, daily $h'F$ values for each month of the years 1966–1998 around the postsunset period are used for this analysis. The daily values allow for better coverage and interpretation of the phenomena. To allow for uniformity in the entire data, the percentage rate was calculated. This is achieved by finding the number of days for which there is no increase in the response of $h'F$ with effect from around 19 LT up till the midnight hours in a particular month divided by the total number of days of continuous hourly data availability in that same month and finding the percentage. For instance,

% monthly rate of inhibition =

$$\frac{\text{days with decrease in } h'F \text{ around 19 LT through the midnight hours in a month}}{\text{total number of days with } h'F \text{ data availability for the same month}}$$

Also,

% annual rate of inhibition =

$$\frac{\text{days with decrease in } h'F \text{ around 19 LT through midnight hours in an entire Year}}{\text{total number of days with } h'F \text{ data availability for the same year}}$$

and

% SC rate of inhibition =

$$\frac{\text{days with decrease in } h'F \text{ around 19 LT through the midnight hours in an entire SC}}{\text{total number of days with } h'F \text{ data availability for the same SC}}$$

The data are manually traced out such that it satisfy the conditions of the $h'F$ response of fourth and eighth of December, 1996 as shown in Figure 10. It is worth mentioning that not all days have complete data set. Hence, days with too much gaps in the data set are not considered. Months constituting years with more of scanty data are also avoided (e.g., 1969 and 1970). Year 1998 had data available for only 2 months, so the annual averages cannot be computed. As a condition for scintillation seeding mechanism, the height profile $h'F$ is expected to continue to rise beyond 18 LT (which is the average period for which the PRE peak

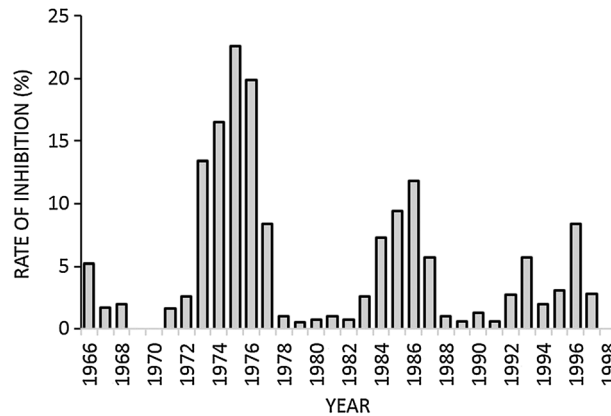


Figure 11. Annual mean magnitudes of the rate of inhibition (measured in percentage) obtained from the response of the height profile.

was observed in this work), since the drift (PRE) around this period pushes the *F* layer height up. At this time, the bottom-side gradient region of the increasing height becomes less stable and is subsequently unable to seed perturbations, leading to the appearance of scintillation effects by the Rayleigh-Taylor (R-T) instability mechanism [de Lima et al., 2015]. Any pattern in the *F* layer altitude that does not support this increase beyond the 18LT like those shown in Figure 10 indicates the condition for characterizing the inhibition of scintillation effect.

Figures 11 and 12 depict the respective percentage annual mean averages and the monthly mean averages for each sunspot cycle characterizing the inhibiting condition. Further, Table 4 summarizes the seasonal inhibiting rate for each sunspot activity period. The following deductions were made from both figures and the table:

1. The inhibition rate maximizes at sunspot minima, increases during sunspot cycle descending phase, decreases during sunspot ascending phase, and minimizes during sunspot maxima for all SCs. This observation is in agreement with the result obtained by de Paula et al. [2003] in which the seeding of scintillation effect maximizes at sunspot maxima at stations in the EIA region.
2. The rate of inhibition is highest during SC 20 and reduces through SC 22.
3. The rate of inhibition of the scintillation effect is higher during the solstices than for the equinox seasons for all SCs. This result is consistent with the observations of some previous works which had earlier reported that scintillation or ESF occurrence is higher in equinox than during solstice. Some of these include Satri et al. [1979], Abdu et al. [1992], Lee et al. [2005], and Sreeja et al. [2009].

4. Summary and Recommendations

The nighttime ionospheric variation in the vertical plasma drift (V_d) was investigated in Ouagadougou in the trough of the EIA region. The data span June 1966–February 1998 extending through three sunspot cycles (SC) 20–22 for different phases and seasons. The annual and 11 year sunspot activity progressions were also considered. Owing to the unavailability of direct measured procedures for obtaining drift velocity in the African sector, the drift was inferred from the time rate of change of the *F* layer height of reflection. The analysis revolved around the two peaks that characterize the drift morphology at nighttime—the evening-time PRE, and the minimum reversal periods.

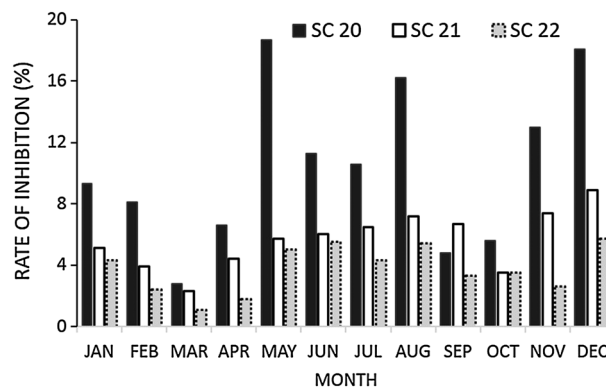


Figure 12. Same as in Figure 11, but for the monthly averages across each sunspot cycle.

Observations show that the mean annual peak magnitudes of V_d during the PRE and minimum reversal periods exhibit the 11 year sunspot cycle evolution with the solar sunspot number (R_z). The correlation coefficients for the PRE peak/ R_z and reversal peak/ R_z observations are 0.987 and 0.848, respectively. The PRE peak magnitude, for the 11 year sunspot cycle seasonal observation, in June solstice (also the lowest) appeared 1 h later when compared with other seasons and found its explanation in the slow growth rate of the Rayleigh-Taylor (R-T) instability mechanism.

Table 4. Average Percentage Rate of Inhibition for the Appearance of Scintillation Effect

Season	Rate of inhibition (%)		
	SC 20	SC 21	SC 22
March equinox	4.70	3.35	1.45
June solstice	14.20	6.35	5.05
September equinox	5.20	5.10	3.40
December solstice	12.13	6.33	3.75

PRE has been found to be related to the ionospheric dynamo system which in turn is connected to neutral wind; since the neutral wind variation is seasonal dependent, it is expected that the same characteristics will be exhibited during the PRE period. PRE magnitude and downward perturbation drifts near dusk were highest/lowest during the equinoctial/solstitial periods. Both the PRE and reversal peak magnitudes exhibit direct sunspot activity dependency. The drift pattern also reveals monthly semiannual asymmetry for all cycles during the PRE event with peaks in March and September/October. One of the remarkable features of this work is the local time presunrise (05 LT) plasma drift enhancement, which is dependent on the phase of sunspot cycle.

Different quantitative magnitudes of the drift were observed for different seasons and activities. Table 5 summarizes the peak magnitudes for the different activity periods and conditions, which are consistent, in parts, with some previous drift results [e.g., Batista et al., 1986; Fejer, 1997; Fejer et al., 1999, 2008; Woodman et al., 2006].

The pattern between different years constituting a sunspot activity period during either the PRE peak event or the postmidnight minimum drift excursion is best described by a fourth-order polynomial equation. Further, the rate of inhibition of the likely appearance of scintillation effect was observed to maximize at sunspot minima and minimize during sunspot maxima for all SCs. The linear drift equation obtained for Ouagadougou for the peak PRE/Rz relationship can be used to predict the annual PRE peak magnitude for stations along the EIA trough in the African sector provided the corresponding annual solar sunspot number is available. It is therefore encouraged that the drift data at this station be integrated into the African regional modeling and consequently in the design of the International Reference Ionosphere drift model.

It is hopeful that the newly installed ground-based All Sky Camera for Night Airglow (OI 630 nm emission) at the National Space Research and Development Agency (NASRDA) centre in Abuja, Nigeria, and the continuous increasing number of GPS stations in the African sector will assist a long way in the direct probing/measurement of scintillation effects in the African sector. The All Sky Camera was installed in May, 2015, and it is the first in Africa.

Table 5. Peak Magnitudes of Plasma Drift for Different Activities and Conditions

Activity/Condition	Plasma Drift (m/s)		
	Peak PRE	Maximum Presunrise	Minimum Downward Excursion
<i>Sunspot Cycle</i>			
SC 20	18.6	5.2	-7.5
SC 21	25.9	5.0	-11.4
SC 22	26.1	0.5	-8.3
<i>Solar Activity Phase</i>			
Maximum/HSA	25.0	5.6	-9.7
Ascending/MSA	13.3	3.0	-4.3
Descending/MSA	9.0	2.1	-4.3
Minimum/LSA	4.5	0.6	-3.9
<i>Seasonal Activity</i>			
March equinox	18.1	4.0	-7.8
June solstice	12.0	1.4	-10.9
September equinox	15.7	2.9	-6.6
December solstice	12.8	3.8	-8.5

Acknowledgments

Authors are grateful to the Ionospheric Laboratory of the Centre National des Télécommunications to Lannion, France, for providing the Ouagadougou ionosonde data in benefit of the scientific community and the National Geophysical Data Centre (NGDC), E/GC 325 Broadway, Boulder, Colorado, USA, 80305–3328 for the provision of the annual Solar Sunspot number (on www.ngdc.noaa.gov/stp/spaceweather/solar_indices/sunspot-numbers). The Ilorin Digisonde data used for the modeling validation was obtained from the University of Ilorin Equatorial Ionospheric Observatory, Nigeria, and was provided by Prof. B. W. Reinisch of Lowell Digisonde International, LLC, Center for Atmospheric Research, University of Lowell Massachusetts, 175 Cabot Street, Suite 200 Lowell, MA 01854, USA (visit giro.uml.edu). We benefited from insightful comments of organizers/participants of the second annual conference of the Nigeria Geophysical Society (NGS) held from 17 to 20 March 2015 at Covenant University, Ota, Nigeria, from where the idea of this paper was conceptualized. The authors appreciate the effort of the Editor, Alan Rodger, and the two reviewers for their insightful comments and suggestions in improving the quality of this paper.

References

- Abdu, M. A., I. S. Batista, and J. A. Bittencourt (1981a), Some characteristics of spread F at the magnetic equatorial station Fortaleza, *J. Geophys. Res.*, *86*, 6836–6842, doi:10.1029/JA086iA08p06836.
- Abdu, M. A., J. A. Bittencourt, and I. S. Batista (1981b), Magnetic declination control of the equatorial F region dynamo electric field development and spread F, *J. Geophys. Res.*, *86*, 11,443–11,446, doi:10.1029/JA086iA13p11443.
- Abdu, M. A., I. S. Batista, and J. H. A. Sobral (1992), A new aspect of magnetic declination control of equatorial spread F and F region dynamo, *J. Geophys. Res.*, *97*, 14,897–14,904, doi:10.1029/92JA00826.
- Abdu, M. A., I. S. Batista, B. W. Reinisch, and A. J. Carrasco (2004), Equatorial F-layer height, evening prereversal electric field, and night E-layer density in the American sector: IRI validation with observations, *Adv. Space Res.*, *34*, 1953–1965.
- Abdu, M. A., P. P. Batista, I. S. Batista, C. G. M. Brum, A. J. Carrasco, and B. W. Reinisch (2006), Planetary wave oscillations in mesospheric winds, equatorial evening prereversal electric field and spread F, *Geophys. Res. Lett.*, *33*, L07107, doi:10.1029/2005GL024837.
- Abdu, M. A., E. A. Kherani, I. S. Batista, and J. H. A. Sobral (2009), Equatorial evening prereversal vertical drift and spread F suppression by disturbance penetration electric fields, *Geophys. Res. Lett.*, *36*, L19103, doi:10.1029/2009GL039919.
- Abdu, M. A., I. S. Batista, C. G. M. Brum, J. Macdougall, A. M. Santos, J. R. Souza, and J. H. A. Sobral (2010), Solar flux effects on the equatorial evening vertical drift and meridional winds over Brazil: A comparison between observational data and the IRI model and the HWM representations, *Adv. Space Res.*, *46*, 1078–1085.
- Adebesin, B. O. (2008), A study of intense magnetic storms development (using Dst signature) and its association with magnetic clouds, *Afr. Rev. Phys.*, *2*(0017), 143–158.
- Adebesin, B. O., J. O. Adeniyi, I. A. Adimula, and B. W. Reinisch (2013a), Low latitude nighttime ionospheric vertical $E \times B$ drifts at African region, *Adv. Space Res.*, *52*(12), 2226–2237, doi:10.1016/j.asr.2013.09.033.
- Adebesin, B. O., J. O. Adeniyi, I. A. Adimula, and B. W. Reinisch (2013b), Equatorial vertical plasma drift velocities and electron densities inferred from ground-based ionosonde measurements during low solar activity, *J. Atmos. Sol. Terr. Phys.*, *97*, 58–64, doi:10.1016/j.jastp.2013.02.010.2013.
- Adebesin, B. O., J. O. Adeniyi, I. A. Adimula, B. W. Reinisch, and K. Yumoto (2013c), F2 layer characteristics and electrojet strength over an equatorial station, *Adv. Space Res.*, *52*(5), 791–800, doi:10.1016/j.asr.2013.05.025.
- Adebesin, B. O., B. J. Adekoya, S. O. Ikubanni, S. J. Adebiji, O. A. Adebesin, B. W. Joshua, and K. O. Olonade (2014), Ionospheric foF2 morphology and response of F2 layer height over Jicamarca during different solar epochs and comparison with IRI-2012 model, *J. Earth Syst. Sci.*, *123*(4), 751–765, doi:10.1007/s12040-014-0435-y.
- Adebesin, B. O., J. O. Adeniyi, I. A. Adimula, O. A. Oladipo, A. O. Olawepo, and B. W. Reinisch (2015), Comparative analysis of nocturnal vertical plasma drift velocities inferred from ground-based ionosonde measurements of hmF2 and h'F, *J. Atmos. Sol. Terr. Phys.*, *122*, 97–107, doi:10.1016/j.jastp.2014.11.
- Adekoya, B. J., and B. O. Adebesin (2015), Ionospheric and solar wind variation during magnetic storm onset and main phase at low- and mid-latitudes, *Acta Geophys.*, *63*(4), 1150–1180, doi:10.1515/acgeo-2015-0020.
- Adeniyi, J. O., and I. A. Adimula (1995), Comparing the F2-layer model of IRI with observations at Ibadan, *Adv. Space Res.*, *15*, 141–144.
- Adeniyi, J. O., and S. M. Radicella (1998), Diurnal variation of ionospheric profile parameters B_0 and B_1 for an equatorial station at low solar activity, *J. Atmos. Sol. Terr. Phys.*, *60*, 381–385.
- Adeniyi, J. O., B. O. Adebesin, I. A. Adimula, O. A. Oladipo, A. O. Olawepo, S. O. Ikubanni, and B. W. Reinisch (2014a), Comparison between African equatorial station ground-based inferred vertical $E \times B$ drift, Jicamarca direct measured drift, and IRI model, *Adv. Space Res.*, doi:10.1016/j.asr.2014.06.014.
- Adeniyi, J. O., I. A. Adimula, B. O. Adebesin, B. W. Reinisch, O. A. Oladipo, A. O. Olawepo, and K. Yumoto (2014b), Quantifying the EEJ current with Ground-based ionosonde inferred vertical $E \times B$ drifts in the morning hours over Ilorin, West Africa, *Acta Geophys.*, *62*(3), 656–678, doi:10.2478/s11600-014-0202-0.
- Batista, I. S., M. A. Abdu, and J. A. Bittencourt (1986), Equatorial F region vertical plasma drifts: Seasonal and longitudinal asymmetries in the American sector, *J. Geophys. Res.*, *91*, 12,055–12,064, doi:10.1029/JA091iA11p12055.
- Bertoni, F., I. S. Batista, M. A. Abdu, B. W. Reinisch, and E. A. Kherani (2006), A comparison of ionosonde vertical drift velocities measured by Digisonde and incoherent scatter radar at the magnetic equator, *J. Atmos. Sol. Terr. Phys.*, *68*, 669–678, doi:10.1016/j.jastp.2006.01.002.
- Bilitza, D., O. K. Obrou, J. O. Adeniyi, and O. Oladipo (2004), Variability of f_oF_2 in the equatorial ionosphere, *Adv. Space Res.*, *34*, 1901–1906, doi:10.1016/j.asr.2004.08.004.
- Bittencourt, J. A., and M. A. Abdu (1981), A theoretical comparison between apparent and real vertical ionization drift velocities in the equatorial F region, *J. Geophys. Res.*, *86*, 2451–2454, doi:10.1029/JA086iA04p02451.
- de Lima, G. R. T., S. Stephany, E. R. de Paula, I. S. Batista, and M. A. Abdu (2015), Prediction of the level of ionospheric scintillation at equatorial latitudes in Brazil using a neural network, *Space Weather*, *13*, 446–457, doi:10.1002/2015SW001182.
- de Paula, E. R., F. S. Rodrigues, K. N. Iyer, I. J. Kantor, M. A. Abdu, P. M. Kintner, B. M. Ledvina, and H. Kintner (2003), Equatorial anomaly effects on GPS scintillations in Brazil, *Adv. Space Res.*, *31*, 749–754, doi:10.1016/S0273-1177(03)00048-6.
- Fejer, B. G. (1997), The electrodynamics of the low-latitude ionosphere: Recent results and future challenges, *J. Atmos. Sol. Terr. Phys.*, *59*, 1456–1482.
- Fejer, B. G. (2002), Low latitude storm time ionospheric electrodynamics, *J. Atmos. Sol. Terr. Phys.*, *64*, 1401–1408.
- Fejer, B. G., and L. Scherliess (1997), Empirical models of storm time equatorial zonal electric fields, *J. Geophys. Res.*, *102*, 24,047–24,056, doi:10.1029/97JA02164.
- Fejer, B. G., L. Scherliess, and E. R. de Paula (1999), Effects of the vertical plasma drift velocity on the generation and evolution of equatorial spread F, *J. Geophys. Res.*, *104*, 19,854–19,869.
- Fejer, B. G., J. W. Jensen, and S. Shin-Yi (2008), Seasonal and longitudinal dependence of equatorial disturbance vertical plasma drifts, *Geophys. Res. Lett.*, *35*, L20106, doi:10.1029/2008GL035584.
- Gnabahou, D. A., F. Ouattara, E. Nanéma, and F. Zougmore (2013), foF2 diurnal variability at African equatorial stations: Dip equator secular displacement effect, *Int. J. Geosci.*, *4*, 1145–1150, doi:10.4236/ijg.2013.48108.
- Huang, X., and B. W. Reinisch (1996), Vertical electron density profiles from the Digisonde ionograms: The average representative profile, *Ann. Geophys.*, *XXXIX*(4), 751–756.
- Ikubanni, S. O., and J. O. Adeniyi (2013), Variation of saturation effect in the ionospheric F2 critical frequency at low latitude, *J. Atmos. Sol. Terr. Phys.*, *100–101*, 24–33, doi:10.1016/j.jastp.2013.03.012.
- Kelley, M. C., R. R. Ilma, and G. Crowley (2009), On the origin of the pre-reversal enhancement of the zonal equatorial electric field, *Ann. Geophys.*, *27*, 2053–2056.
- Klenzing, J., F. Simoes, S. Ivanov, D. Bilitza, R. A. Heelis, and D. Rowland (2013), Performance of the IRI-2007 model for equatorial topside ion density, *Adv. Space Res.*, *52*(10), 1780–1790.

- Lee, C. C., J. Y. Liu, B. W. Reinisch, W. S. Chen, and F. D. Chu (2005), The effects of the pre-reversal E \times B drift, the EIA asymmetry, and magnetic activity on the equatorial spread F during solar maximum, *Ann. Geophys.*, *23*, 745–751.
- Li, G., B. Ning, M. A. Abdu, X. Yue, L. Liu, W. Wan, and L. Hu (2011), On the occurrence of postmidnight equatorial F region irregularities during the June solstice, *J. Geophys. Res.*, *116*, A04318, doi:10.1029/2010JA016056.
- Liu, J., B. Zhao, and L. Liu (2010), Time delay and duration of ionospheric total electron content responses to geomagnetic disturbances, *Ann. Geophys.*, *28*, 795–805.
- Liu, L., X. Luan, W. Wan, J. Lei, and B. Ning (2004), Solar activity variations of equivalent winds derived from global ionosonde data, *J. Geophys. Res.*, *109*, A12305, doi:10.1029/2004JA010574.
- Martinis, C. R., M. J. Mendillo, and J. Aarons (2005), Toward a synthesis of equatorial spread F onset and suppression during geomagnetic storms, *J. Geophys. Res.*, *110*, 7306–7319, doi:10.1029/2003JA010362.
- Mazaudier, C., and M. Blanc (1982), Electric currents above Saint-Santin; Part II: Model, *J. Geophys. Res.*, *87*, 2465–2480, doi:10.1029/JA087iA04p02465.
- Mazaudier, C., M. Blanc, E. Nielsen, and Z. Min-Yun (1984), Latitudinal profile of the magnetospheric convection electric field at ionospheric altitudes from a chain of magnetic and radar data, *J. Geophys. Res.*, *89*, 375–381, doi:10.1029/JA089iA01p00375.
- Nayar, S. R. P., T. J. Mathew, C. V. Sreehari, S. G. Sumod, C. V. Devasia, S. Ravindran, V. Sreeja, T. Kumar Pant, and R. Sridharan (2009), Electrodynamics of the equatorial F-region ionosphere during pre-sunrise period, *Ann. Geophys.*, *27*, 107–111.
- Obrou, O. K. (2008), Ionospheric scintillation and equatorial anomaly Paper presentation at African IHY School AFRIS, 10 – 21 November, 2008, Enugu, Nigeria.
- Oyekola, O. S. (2011), Comparison of foF2 with IRI model and equatorial vertical drifts, *Adv. Space Res.*, *48*, 1318–1326.
- Quattara, F., and C. Amory-Mazaudier (2012), Statistical study of the equatorial F2 layer critical frequency at Ouagadougou during solar cycles 20, 21, and 22, using Legrand and Simon's classification of geomagnetic activity, *J. Space Weather Space Clim.*, *2*, 1–10.
- Quattara, F., C. Amory-Mazaudier, R. Fleury, D. P. Lassudrie, and M. Petitdidier (2009), West Africa equatorial ionospheric parameters climatology based on Ouagadougou ionosonde station data from June 1966 to February 1998, *Ann. Geophys.*, *27*, 2503–2514.
- Rabiu, A. B., A. I. Mamukuyomi, and E. O. Joshua (2007), Variability of equatorial ionosphere inferred from geomagnetic field measurements, *Bull. Astron. Soc. India*, *35*, 607–618.
- Rabiu, A. B., O. E. Abe, and J. O. Adeniyi (2012), Variability of the vertical extent of ionospheric E-layer over a station within equatorial anomaly region, *Indian J. Radio Space Phys.*, *41*, 536–542.
- Richmond, A. D., C. Peymirat, and R. G. Roble (2003), Long-lasting disturbances in the equatorial ionospheric electric field simulated with a coupled magnetosphere-ionosphere-thermosphere model, *J. Geophys. Res.*, *108*(A3), 1118, doi:10.1029/2002JA009758.
- Rishbeth, H. (1971), Polarization fields produced by winds in the equatorial F-region, *Planet. Space Sci.*, *19*, 357–369.
- Rishbeth, H. (1981), The F-region dynamo, *J. Atmos. Terr. Phys.*, *43*, 387–392.
- Rishbeth, H., and O. K. Garriott (1969), *Introduction to Ionospheric Physics*, Academic Press, New York.
- Rishbeth, H., I. C. F. Muller-Wodarg, L. Zou, T. J. Fuller-Rowell, G. H. Millward, R. J. Moffett, D. W. Idenden, and A. D. Aylward (2000), Annual and semiannual variations in the ionospheric F2-layer: II Physical discussion, *Ann. Geophys.*, *18*, 945–956.
- Santos, A. M., M. A. Abdu, J. H. A. Sobral, D. Koga, P. A. B. Nogueira, and C. M. N. Candido (2012), Strong longitudinal difference in ionospheric responses over Fortaleza (Brazil) and Jicamarca (Peru) during the January 2005 magnetic storm, dominated by northward IMF, *J. Geophys. Res.*, *117*, A08333, doi:10.1029/2012ja017604.
- Santos, A. M., M. A. Abdu, J. H. A. Sobral, M. Mascarenhas, and P. A. B. Nogueira (2013), Equatorial evening prereversal vertical drift dependence on solar EUV flux and F10.7 index during quiet and disturbed periods over Brazil, *J. Geophys. Res. Space Physics*, *118*, 1–10, doi:10.1002/jgra.50438.
- Satri, J. H., B. S. Murthy, and K. Sasidharan (1979), Range and frequency spread-F at Kodaikanal, *Ann. Geophys.*, *35*, 153–158.
- Simon, P. A., and J. P. Legrand (1989), Solar cycle and geomagnetic activity: A review for geophysicists. Part II. The solar sources of geomagnetic activity and their links with sunspot cycle activity, *Ann. Geophys.*, *7*(6), 579–594.
- Sreeja, V., C. V. Devasia, S. Ravindran, and T. K. Pant (2009), Observational evidence for the plausible linkage of Equatorial Electrojet (EEJ) electric field variations with the post sunset F-region electrodynamics, *Ann. Geophys.*, *27*, 4229–4238.
- Su, S. Y., C. K. Chao, and C. H. Liu (2009), Cause of different local time distribution in the post-sunset equatorial ionospheric irregularity occurrences between June and December solstices, *J. Geophys. Res.*, *114*, A04321, doi:10.1029/2008JA013858.
- Uemoto, J., T. Maruyama, S. Saito, M. Ishii, and R. Yushima (2010), Relationship between presunset electrojet strength, PRE and ESF onset, *Ann. Geophys.*, *28*, 449–454.
- Woodman, R. F., J. L. Chau, and R. R. Ilma (2006), Comparison of ionosonde and incoherent scatter drift measurements at magnetic equator, *Geophys. Res. Lett.*, *33*, L01103, doi:10.1029/2005GL023692.
- Zerbo, J. L., C. Amory Mazaudier, F. Quattara, and J. D. Richardson (2012), Solar wind and geomagnetism: toward a standard classification of geomagnetic activity from 1868 to 2009, *Ann. Geophys.*, *30*, 421–426.